crystals

Article

Effects of Uniaxial Tensile Strain on Mechanical Properties of Al_6MgNb: A First-Principles Study

Lihua Zhang [1,†], Jijun Li [2,*,†], Jing Zhang [2,*], Yanjie Liu [2] and Lin Lin [3,*]

[1] School of Science, Shanghai Maritime University, Shanghai 201306, China; dapperzhanglh@163.com
[2] School of Mechanical and Energy Engineering, Shanghai Technical Institute of Electronics and Information, Shanghai 201411, China; hnlylyj@163.com
[3] College of Science, Inner Mongolia University of Technology, Hohhot 010051, China
[*] Correspondence: ji_jun_li@163.com (J.L.); zhangjing_hust@163.com (J.Z.); linlintuoya@163.com (L.L.)
[†] These authors contributed equally to this work and should be considered co-first authors.

Abstract: The effects of uniaxial tensile strain in the *x* direction (ε_x) on the mechanical properties of the Al_6MgNb compound were explored by carrying out first-principles calculations based on the density functional theory (DFT). The calculation results showed that the Al_6MgNb compound was stable in mechanics at a uniaxial tensile strain range of 0–12%. The shear modulus *G*, bulk modulus *B* and Young's modulus *E* of the Al_6MgNb compound all decreased as the uniaxial tensile strain ε_x grew from 0 to 12%, exhibiting the negative sensitivities of elastic moduli to uniaxial tensile strain. The Poisson ratio ν of the Al_6MgNb compound grew with the increase in uniaxial tensile strain ε_x from 0 to 7%, exhibiting the positive sensitivity of Poisson's ratio to uniaxial tensile strain, but it decreased as the uniaxial tensile strain ε_x increased from 7% to 12%, exhibiting its negative sensitivity to the uniaxial tensile strain. The Al_6MgNb compound possesses the optimal toughness under a uniaxial tensile strain ε_x of 7% because of the largest value of ν. The Vickers hardness H_V of the Al_6MgNb compound decreased first and then remained stable with the growth in uniaxial tensile strain ε_x from 0 to 12%, exhibiting the significant negative sensitivity of the Vickers hardness to tensile uniaxial strain at a strain range of 0–7%. The ratio of the bulk modulus *B* to the elastic shear modulus *G* (i.e., *B/G*) increased first and then decreased with the growth in uniaxial tensile strain ε_x from 0 to 12%. The highest ductility is achieved for the Al_6MgNb compound at a strain ε_x of 7% because of the largest value of *B/G*. The compression anisotropy percentage A_B, shear anisotropy percentage A_G and the universal anisotropy index A_U of the Al_6MgNb compound all increased as the uniaxial tensile strain ε_x increased from 0 to 12%, exhibiting the positive sensitivity of elastic anisotropy to the uniaxial tensile strain. Our study suggested that the mechanical properties of the Al_6MgNb compound can be influenced and regulated by applying proper uniaxial tensile strain. These findings can provide a favorable reference to the study on mechanical performance of Al-Mg-based materials by means of strain modulation.

Keywords: Al_6MgNb compound; mechanical properties; uniaxial tensile strain; first-principles calculation

check for updates

Citation: Zhang, L.; Li, J.; Zhang, J.; Liu, Y.; Lin, L. Effects of Uniaxial Tensile Strain on Mechanical Properties of Al_6MgNb: A First-Principles Study. *Crystals* **2023**, *13*, 1458. https://doi.org/10.3390/cryst13101458

Academic Editor: Umberto Prisco

Received: 28 August 2023
Revised: 19 September 2023
Accepted: 26 September 2023
Published: 2 October 2023

1. Introduction

Owing to their light weight, formability, good resistance to corrosion, great weldability, affordability and excellent recyclability, aluminum-magnesium (Al-Mg)-based compounds and alloys are extensively applied in aerospace, automobile, marine, electronics and civil fields [1–3]. Nevertheless, Al-Mg-based materials also possess a relatively low strength, which greatly limits their practical applications [4,5]. Therefore, it is extremely important to enhance the mechanical performance of these kinds of materials. The addition of elements, for example, Zr, Er, Sc, Zn, Ag and Cu, can upgrade the mechanical performance of Al-Mg-based materials [6–9]. Researchers have shown that Niobium (Nb) also has the potential to enhance the mechanical performance of some compounds and alloys [10–14].

However, there is a lack of research regarding the mechanical behaviors of Al-Mg-based materials with the addition of Nb.

In recent years, strain engineering, which represents an effective and promising strategy, has been shown to regulate the functional properties of materials via modulating the lattice strain [15,16]. Dong et al. [17] studied the characteristic deformation behavior of AA6014-T4P aluminum alloy via cyclic loading. It was found that this material exhibited a softening behavior in the process of tensile loading while the compressive pre-strain was imposed, but this phenomenon did not appear while the loading sequence was inverted. Tan et al. [18] explored the mechanical behaviors of $AlSi_2Sc_2$ under uniaxial tensile strain by carrying out first-principles calculations on the basis of density functional theory (DFT). The findings demonstrated that the calculated elastic moduli of $AlSi_2Sc_2$ decreased with the growth in uniaxial tensile strain, whereas its brittleness remained unchanged when the strain was exerted. Rasidul Islam et al. [19] studied the mechanical behaviors induced by the strain of the $CsGeBr_3$ compound via first-principles calculations on the basis of DFT. The results indicated that the elastic moduli (including the shear modulus, bulk modulus and Young's modulus) went up with the growth in compressive strain but went down with the growth in tensile strain. The brittleness of $CsGeBr_3$ went up with the growth in compressive strain, whereas it exhibited noticeable ductility when the tensile strain was greater than 2%. Sun et al. [20] studied the influence of pre-strain at ambient and cryogenic temperatures on the microstructure evolution and sulfide stress corrosion cracking (SSCC) of 304 stainless steel. It was found that the 304 stainless steel exhibited exceedingly strong SSCC susceptibility, and the SSCC susceptibility grew with the increasing pre-strain as a consequence of the speedup of both the anodic dissolution and hydrogen embrittlement. However, as far as we know, the existing studies rarely involve research into the mechanical behaviors of Al-Mg-based compounds with Nb addition under the applied strain.

The purpose of this study is to explore the effects of uniaxial tensile strain on the mechanical properties of the Al_6MgNb compound via first-principle calculations based on the DFT. We hope that our findings will provide some useful information for the application of strain engineering in mechanical performance modulation of Al-Mg-based materials.

2. Methodology

In the present work, we executed the first principles on the basis of DFT to explore the mechanical stability, elastic properties, hardness, ductility and elastic anisotropy of the Al_6MgNb compound under the various uniaxial tensile strains. The Cambridge Sequence Total Energy Packet (CASTEP) code was utilized, in which the ultrasoft pseudopotential was employed for the interaction between valence electrons and ion core [21]. The generalized gradient approximation in the Perdew–Burke–Ernzerhof scheme (GGA-PBE) was conducted to represent the exchange-correlation energy [22]. During the geometry optimization, the total energy convergence was set as 5×10^{-6} eV/atom, the maximum force was set as 0.01 eV/Å, the maximum stress was set as 0.02 GPa and the maximum displacement was set as 5×10^{-4} Å. To ensure high calculation precision, the plane-wave cutoff energy was set to 600 eV, and the Brillouin zone sampling was performed with a $3 \times 6 \times 6$ k-point mesh. The optimized structure of the Al_6MgNb supercell is shown in Figure 1. The supercell includes eight atoms in total (including one Nb atom, six Al atoms and one Mg atom). Green, gray and orange spheres stand for Nb, Al and Mg atoms, respectively.

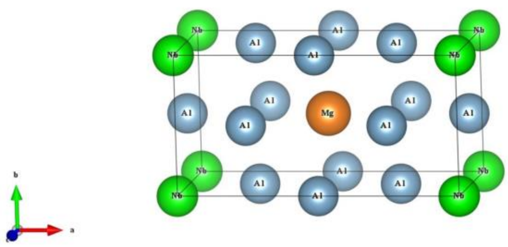

Figure 1. Optimized structure of the Al_6MgNb supercell.

3. Results and Discussion

3.1. Mechanical Stability

The elastic stiffness constants C_{ij} are the fundamental parameters to characterize the mechanical behaviors of the solid material in the practical engineering, which not only provide essential information about how a solid material reacts to an external force, but also give the relation between mechanical and dynamical behaviors [23]. There were nine independent effective parameters (C_{11}, C_{12}, C_{13}, C_{22}, C_{23}, C_{33}, C_{44}, C_{55} and C_{66}) in the elastic stiffness matrix of the Al_6MgNb compound due to the orthorhombic symmetry [24]. Table 1 shows the calculated elastic stiffness constants C_{ij} of the Al_6MgNb compound under various uniaxial tensile strains in the x direction (ε_x) from first-principles calculations. In general, the stability in the mechanics of a solid material can be assessed using Born–Huang's dynamical theory of crystal lattices [25,26]. For an orthorhombic crystal, the mechanical stability requires the elastic stiffness constants C_{ij} to meet the conditions below [27]:

$$\begin{cases} C_{ii} > 0 \\ C_{22} + C_{11} - 2C_{12} > 0 \\ C_{33} + C_{11} - 2C_{13} > 0 \\ C_{33} + C_{22} - 2C_{23} > 0 \\ C_{33} + C_{22} + C_{11} + 2(C_{23} + C_{13} + C_{12}) > 0 \end{cases} \quad (1)$$

Table 1. Calculated elastic stiffness constants C_{ij} (in GPa) of the Al_6MgNb compound under various uniaxial tensile strains in the x direction (ε_x).

ε_x (%)	C_{11} (GPa)	C_{12} (GPa)	C_{13} (GPa)	C_{22} (GPa)	C_{23} (GPa)	C_{33} (GPa)	C_{44} (GPa)	C_{55} (GPa)	C_{66} (GPa)
0	177.30	49.321	49.251	165.257	65.73	165.162	64.91	30.5332	30.5334
1%	162.48	41.6166	41.6164	154.9274	69.16	154.9228	64.49	23.9430	23.9367
2%	150.01	39.14	39.13	145.04	74.79	145.04	62.65	20.7198	20.7206
3%	136.86	37.15	37.15	135.66	79.08	135.67	60.15	17.3070	17.3071
4%	124.25	35.10	35.11	128.24	81.94	128.21	58.02	14.1912	14.1887
5%	112.70	32.72	32.77	122.86	83.35	122.86	56.99	11.6577	11.6580
6%	100.41	29.65	29.65	119.35	83.52	119.34	57.65	9.6618	9.6604
7%	92.88	26.34	26.35	117.63	82.77	117.65	60.12	8.1493	8.1474
8%	83.76	23.41	23.40	117.24	81.16	117.27	63.78	6.8150	6.8164
9%	70.03	21.31	21.33	117.09	78.64	117.13	67.36	5.4851	5.4862
10%	49.76	20.89	20.91	116.25	75.28	116.17	69.62	4.1904	4.1915
11%	25.86	21.97	22.00	114.58	71.32	114.61	70.28	3.2110	3.2132
12%	5.63	22.52	22.53	113.65	67.71	113.66	69.86	2.9094	2.9037
13%	−4.33	20.12	20.18	113.97	65.18	113.87	68.94	3.6312	3.6562

Through the analysis of the elastic constants C_{ij} of the Al_6MgNb compound shown in Table 1, it was found that the C_{ij} satisfied the mechanical stability criteria at a uniaxial tensile strain ε_x range of 0–12%, but they could not satisfy the above criteria when the strain ε_x was more than 12%. Therefore, the Al_6MgNb compound was mechanically stable at the uniaxial tensile strain range of 0–12%. This study only focuses on the mechanical properties of the Al_6MgNb compound at the uniaxial tensile strain range of 0–12%.

3.2. Elastic Properties of Polycrystalline

In general, the elastic properties of polycrystalline have more important realistic meaning than that of monocrystal [28]. The elastic properties of polycrystalline are represented via the shear modulus (denoted by the G), bulk modulus (denoted by the B) Young's modulus (denoted by the E) and Poisson's ratio (denoted by the ν).

The theoretical elastic moduli of polycrystalline can be obtained via the independent elastic stiffness constants C_{ij} based on first-principles calculations, and the lower and upper bounds are generally signified via the Reuss (R) and Voigt (V) methods, respectively. The shear modulus G and bulk modulus B via the Reuss method can be calculated as below [29]:

$$G_{\mathrm{R}} = \frac{15}{3(S_{66}+S_{55}+S_{44})+4(S_{33}+S_{22}+S_{11})-4(S_{23}+S_{13}+S_{12})} \quad (2)$$

$$B_{\mathrm{R}} = \frac{1}{S_{33}+S_{22}+S_{11}+2(S_{23}+S_{13}+S_{12})} \quad (3)$$

where S_{ij} are the elastic compliance coefficients.

The shear modulus G and bulk modulus B via the Voigt method can be expressed as below [29]:

$$G_{\mathrm{V}} = \frac{C_{66}+C_{55}+C_{44}}{5} + \frac{C_{33}+C_{22}+C_{11}-C_{23}-C_{13}-C_{12}}{15} \quad (4)$$

$$B_{\mathrm{V}} = \frac{C_{33}+C_{22}+C_{11}+2(C_{23}+C_{13}+C_{12})}{9} \quad (5)$$

The Voigt–Reuss–Hill (VRH) average, which is the arithmetic mean of the Reuss and Voigt bounds, is regarded as the optimum estimation of the theoretical elastic modulus for the polycrystalline, as follows [29]:

$$G = \frac{G_{\mathrm{R}}+G_{\mathrm{V}}}{2} \quad (6)$$

$$B = \frac{B_{\mathrm{R}}+B_{\mathrm{V}}}{2} \quad (7)$$

Young's modulus E and Poisson's ratio ν of the polycrystalline can be determined using the shear modulus G and bulk modulus B, and the calculation formulas are given as below [29]:

$$E = \frac{9GB}{G+3B} \quad (8)$$

$$\nu = \frac{3B-2G}{2G+6B} \quad (9)$$

Table 2 and Figure 2 show the calculated shear modulus G, bulk modulus B, Young's modulus E and Poisson's ratios ν of the Al_6MgNb compound under various uniaxial tensile strains ε_{x}.

Table 2. Calculated elastic moduli (G, B and E) and Poisson's ratios ν of the Al_6MgNb compound under various uniaxial tensile strains in the x direction (ε_{x}).

ε_{x} (%)	G (GPa)	B (GPa)	E (GPa)	ν
0	45.575	92.700	117.473	0.289
1%	40.000	86.235	103.931	0.299
2%	35.840	82.625	93.938	0.311
3%	31.450	78.895	83.284	0.324
4%	27.585	75.210	73.740	0.337
5%	24.615	71.535	66.247	0.346
6%	22.500	67.350	60.736	0.350
7%	21.360	63.955	57.661	0.350
8%	20.510	60.405	55.274	0.347
9%	19.365	55.925	52.083	0.345
10%	17.615	49.550	47.246	0.341
11%	15.590	39.805	41.369	0.327
12%	11.620	25.500	30.263	0.302

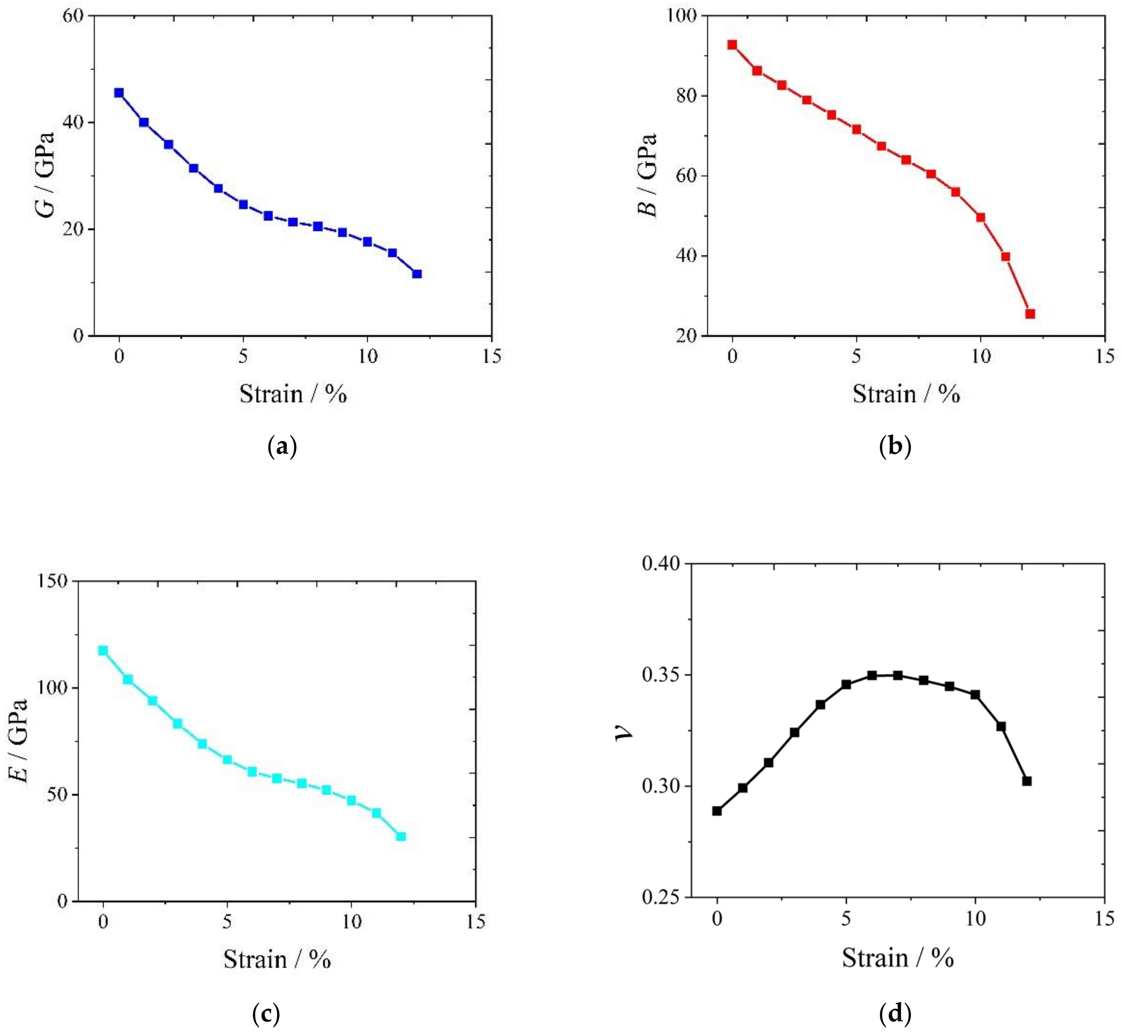

Figure 2. Variation in the elastic moduli (*B*, *G* and *E*) and Poisson's ratio *ν* of the Al_6MgNb compound with uniaxial tensile strain in *x* direction (ε_x): (**a**) shear modulus *G* vs. uniaxial tensile strain ε_x; (**b**) bulk modulus *B* vs. uniaxial tensile strain ε_x; (**c**) Young's modulus *E* vs. uniaxial tensile strain ε_x; (**d**) Poisson's ratio *ν* vs. uniaxial tensile strain ε_x.

The shear modulus *G* reflects the ability of a material to resist the shear deformation. The larger *G* implies the larger shear resistance of a material. The graph in Figure 2a shows the calculated shear modulus *G* of the Al_6MgNb compound under various uniaxial tensile strains ε_x. It is clear that with the growth in strain ε_x from 0 to 12%, the shear modulus *G* decreased from 45.575 GPa to 11.620 GPa. The shear modulus *G* dropped by 74.5%, which suggested that the shear resistance was considerably affected by the uniaxial tensile strain. The Al_6MgNb compound possesses the minimum shear resistance at the strain ε_x of 12% because of the minimum value of *G*. The bulk modulus *B* denotes the resistance of the substance to volumetric compression from applied pressure. The graph in Figure 2b shows the calculated bulk modulus *B* for the Al_6MgNb compound under various uniaxial tensile strains ε_x. It is clear that with the growth in strain ε_x from 0 to 12%, the bulk modulus *B* decreased from 92.7 GPa to 25.5 GPa. The bulk modulus *B* dropped by 72.5%, which exhibited the significant negative sensitivity of bulk modulus *B* to the uniaxial tensile strain. The Al_6MgNb compound has the highest incompressibility at the relaxed state because of the maximum value of *B*, but it is the most compressible at the strain ε_x of 12% because of the minimum value of *B*. Young's modulus *E* characterizes the stiffness of the solid materials. The larger *E* means the higher stiffness of a solid material. The graph in Figure 2c presents the calculated Young's modulus *E* of the Al_6MgNb compound under various uniaxial tensile strains ε_x. It is clear that Young's modulus E decreased with the increase in strain ε_x. When the Al_6MgNb compound was at the unstrained state, Young's modulus E was 117.473 GPa. While the strain ε_x was up to 12%, Young's modulus E decreased to 30.263 GPa. Young's modulus E dropped by 74.2%, exhibiting the significant negative sensitivity of Young's modulus E to the uniaxial tensile strain. The Al_6MgNb compound has the maximum stiffness at the relaxed state because of the maximum value of E, but it represents the minimum stiffness at the strain ε_x of 12% because of the minimum value of E. The change tendencies of elastic moduli (G, B and E) for the Al_6MgNb compound according to the uniaxial tensile strain are analogous to those of $AlSi_2Sc_2$ [18]. The graph in Figure 2d shows the calculated Poisson's ratio ν for the Al_6MgNb compound at various uniaxial tensile strains ε_x. It is clear that with the growth in uniaxial tensile strain ε_x from 0 to 7%, Poisson's ratio ν of the Al_6MgNb compound increased from 0.289 to the maximum value of 0.34974. However, with the increase in strain ε_x from 7 to 12%, Poisson's ratio ν decreased from the maximum of 0.34974 to 0.302. The Al_6MgNb compound obtained the maximum ν value at the strain ε_x of 7%, suggesting that the Al_6MgNb compound possesses the optimal toughness at the strain ε_x of 7%. In general, the Poisson ratio ranged from -1 to 0.5, meaning that the material is relatively stable under shear deformation. From the graph in Figure 2d, it is clear that the Poisson ratio of the Al_6MgNb compound was between 0.289 and 0.350, which is within the range of -1 to 0.5, implying that the Al_6MgNb compound is a stable linear elastic solid at a range of uniaxial tensile strain ε_x between 0 and 12%.

By comparing Figure 2a–d, we can see that as the uniaxial tensile strain ε_x increased from 0 to 12%, the elastic moduli (G, B and E) of the Al_6MgNb compound declined monotonically, but the Poisson ratio ν increased first and then decreased.

3.3. Hardness and Ductility

As a key mechanical parameter of a solid material, hardness describes its ability to withstand surface invasion from external objects, and it has an important influence on the practical application of functional materials. Considering that the shear modulus G and bulk modulus B can be determined by means of the first-principles calculations, a relatively simple semi-empirical model established by Chen et al. can be used to evaluate the Vickers hardness H_V of a solid material, and its formula is as follows [30]:

$$H_V = 1.887k^{1.717}G^{0.591}, \quad k = G/B \tag{10}$$

This semi-empirical model can correctly predict the hardness of a variety of polycrystalline materials and bulk metallic glasses.

The inherent ductility or brittleness of the solid material correlates with the ratio of the bulk modulus B to the shear modulus G (i.e., B/G). In the event that the B/G is greater than 1.75, the material exhibits ductility in nature, but if the B/G is less than 1.75, it characterizes the brittleness feature [31,32].

Table 3 and Figure 3 show the calculated Vickers hardness H_V and the ratio B/G of the Al_6MgNb compound under various uniaxial tensile strains in the x direction (ε_x).

Table 3. Calculated Vickers hardness H_V and the ratio *B/G* of the Al_6MgNb compound under various uniaxial tensile strains in the *x* direction (ε_x).

ε_x (%)	H_V (GPa)	*B/G*
0	7.852	2.034
1%	6.791	2.156
2%	5.883	2.305
3%	4.933	2.509
4%	4.141	2.726
5%	3.593	2.906
6%	3.291	2.993
7%	3.190	2.994
8%	3.176	2.945
9%	3.141	2.888
10%	3.063	2.813
11%	3.192	2.553
12%	3.203	2.194

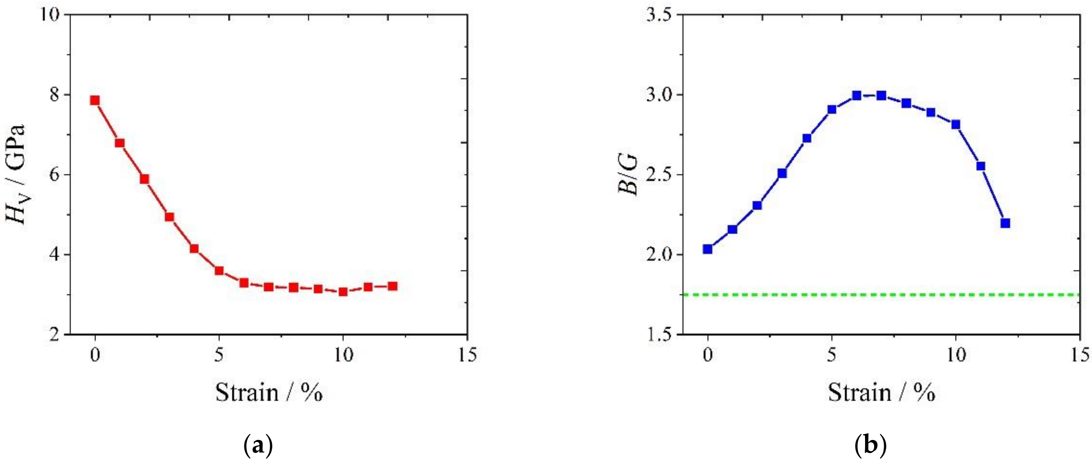

Figure 3. Variation in Vickers hardness H_V and ratio *B/G* of the Al_6MgNb compound with uniaxial tensile strain in the *x* direction (ε_x): (**a**) H_V vs. strain ε_x; (**b**) *B/G* vs. strain ε_x.

From the graph in Figure 3a, with the growth in uniaxial tensile strain ε_x from 0 to 7%, the Vickers hardness H_V of the Al_6MgNb compound decreased rapidly from 7.852 GPa to 3.190 GPa. The Vickers hardness H_V was down by 59.4%, exhibiting the significant negative sensitivity of the Vickers hardness H_V to the tensile uniaxial strain. However, the Vickers hardness H_V changed little with the growth in uniaxial tensile strain ε_x from 7% to 12%.

From the graph in Figure 3b, with the growth in uniaxial tensile strain ε_x from 0 to 12%, the ratio *B/G* of the Al_6MgNb compound increased from 2.034 to the maximum of 2.994, and then decreased to 2.194. The ratio *B/G* corresponding to the green dashed-line in Figure 3b is 1.75. Obviously, in the strain ε_x between 0 and 12%, the ratio *B/G* was greater than 1.75, which implied that the Al_6MgNb compound exhibited ductility. The Al_6MgNb compound obtained the highest ductility at the strain ε_x of 7% because of the maximum *B/G* value of 2.994. Therefore, an improved ductility can be achieved for the Al_6MgNb compound by applying appropriate uniaxial tensile strain.

3.4. Elastic Anisotropy

The elastic anisotropy of a solid material can be depicted by means of the elastic anisotropy indexes. The elastic anisotropy indexes include compression anisotropy percentage (denoted by the A_B), shear anisotropy percentage (denoted by the A_G) and the universal anisotropy index A_U (denoted by the A_U), and their calculation formulas are as below [28]:

$$\begin{cases} A_B = \frac{B_V - B_R}{B_V + B_R} \\ A_G = \frac{G_V - G_R}{G_V + G_R} \\ A_U = 5\frac{G_V}{G_R} + \frac{B_V}{B_R} - 6 \end{cases} \quad (11)$$

where B_V and G_V are determined via Voigt approximation, and B_R and G_R are determined via Reuss approximation.

When the elastic anisotropy indexes have a relationship of $A_B = A_G = A_U = 0$, the material has elastic isotropy. Otherwise, it exhibits elastic anisotropy, and the greater the difference between the elastic anisotropy indexes and the 0 is, the higher the degree of elastic anisotropy becomes.

Table 4 and Figure 4 present the calculated elastic anisotropy indexes (A_B, A_G and A_U) of the Al_6MgNb compound under various uniaxial tensile strains ε_x.

Table 4. Calculated elastic anisotropy indexes (A_B, A_G and A_U) of the Al_6MgNb compound under various uniaxial tensile strains in the *x* direction (ε_x).

ε_x (%)	A_B	A_G	A_U
0%	0	5.672%	0.601
1%	0.133%	9.500%	1.052
2%	0.345%	11.468%	1.302
3%	0.691	14.277%	1.679
4%	1.197%	17.890%	2.203
5%	1.908%	21.999%	2.859
6%	3.073%	26.578%	3.683
7%	4.073%	31.695%	4.725
8%	5.620%	37.348%	6.080
9%	8.646%	43.868%	8.004
10%	15.782%	51.064%	10.810
11%	35.561%	58.178%	15.015
12%	99.765%	99.139%	2000.000

From the graph in Figure 4a, as the uniaxial tensile strain ε_x increased from 0 to 12%, the compression anisotropy percentage A_B increased from 0 to 99.765%, and its rising slope increased suddenly when the strain ε_x was more than 9%. The Al_6MgNb compound represented the highest degree of compression anisotropy at the uniaxial tensile strain ε_x of 12% because of the largest A_B value, which was close to 1. The change in shear anisotropy percentage A_G according to the uniaxial tensile strain ε_x has an analogous trend to that of A_B, as shown in the graph in Figure 4b. With the growth in uniaxial tensile strain ε_x from 0 to 12%, A_G increased from 5.672% to 99.139%. The Al_6MgNb compound represented the highest degree of shear anisotropy at the uniaxial tensile strain ε_x of 12% because of the largest A_G value, which was close to 1. The universal anisotropy index A_U characterizes anisotropy more exactly because not only the shear modulus G but also the bulk modulus B is considered in A_U. As illustrated in the graph in Figure 4c, the variation in universal anisotropy index A_U with uniaxial tensile strain ε_x also has an analogous trend to that of A_B. When the strain ε_x was 12%, A_U reached 2000, reflecting the highest elastic anisotropy. Therefore, the elastic anisotropy indexes (A_B, A_G and A_U) of the Al_6MgNb compound went up with the growth in strain ε_x, displaying their positive sensitivities to the uniaxial tensile strain. The change tendencies of elastic anisotropy indexes for the Al_6MgNb compound according to uniaxial tensile strain are analogous to those of $MoSi_2$ [23]. The degree of elastic anisotropy of the Al_6MgNb compound was enhanced by the uniaxial tensile strain, and the Al_6MgNb compound exhibited stronger elastic anisotropy under higher uniaxial tensile strain.

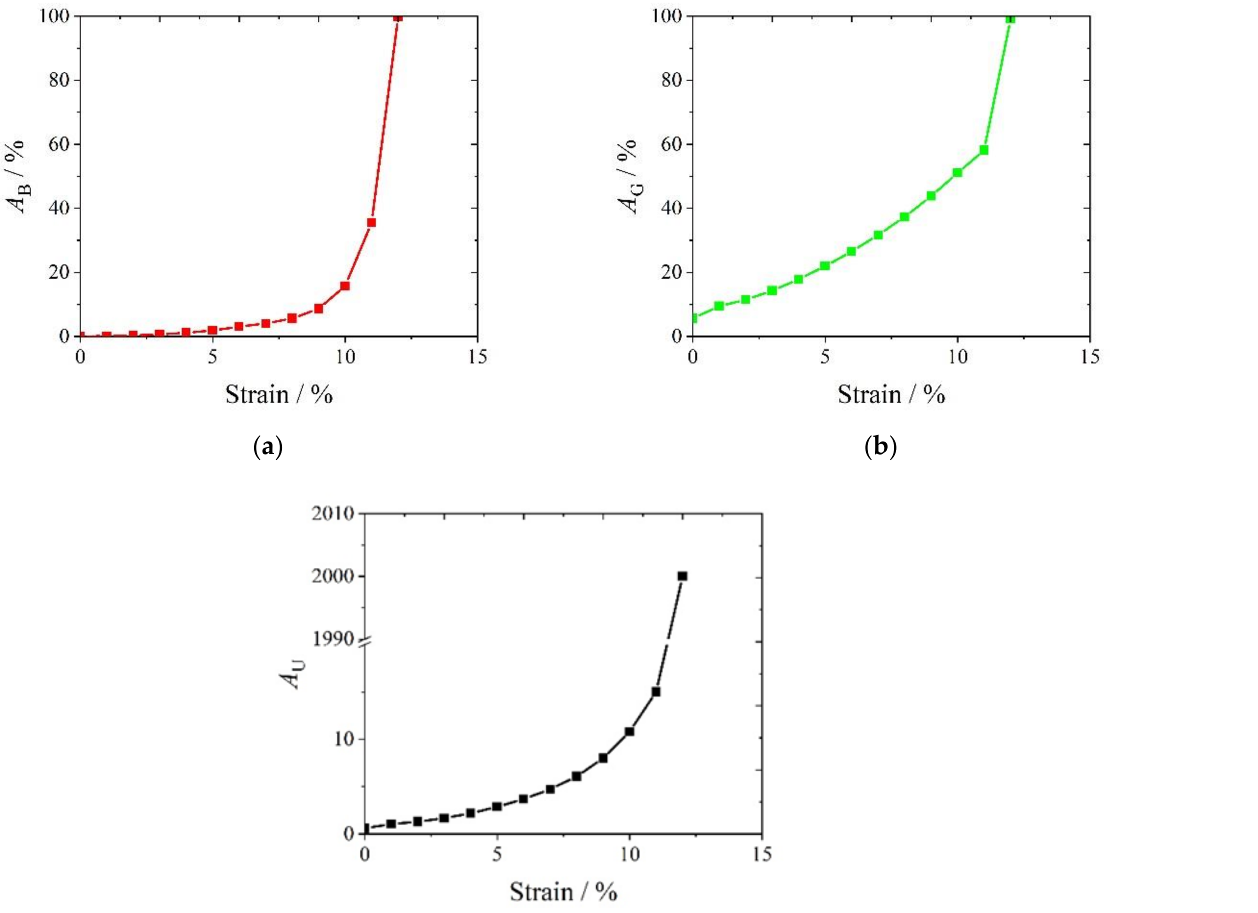

(**c**)

Figure 4. Variation in elastic anisotropy indexes of the Al_6MgNb compound as uniaxial tensile strain in the *x* direction (ε_x): (**a**) compression anisotropy percentage A_B vs. strain ε_x; (**b**) shear anisotropy percentage A_G vs. strain ε_x; (**c**) universal anisotropy index A_U vs. strain ε_x.

4. Conclusions

On the whole, first-principles calculations were utilized to explore the mechanical properties of the Al_6MgNb compound under the uniaxial tensile strain ε_x. The effects of uniaxial tensile strain on the mechanical stability, elastic properties, hardness, ductility and elastic anisotropy for the Al_6MgNb compound were analyzed. The following conclusions can be reached:

1. The Al_6MgNb compound was stable in mechanics at a uniaxial tensile strain range of 0–12%, but it was mechanically unstable while the strain ε_x was greater than 12%.
2. The shear modulus *G*, bulk modulus *B* and Young's modulus *E* of the Al_6MgNb compound all went down with the growth in strain ε_x, exhibiting the negative sensitivities of its moduli to the uniaxial tensile strain. Thereby, the shear resistance, incompressibility and stiffness of the Al_6MgNb compound all went down with the growth in uniaxial tensile strain.
3. As the uniaxial tensile strain ε_x grew from 0 to 7%, the Poisson ratio ν of the Al_6MgNb compound went up, showing the positive sensitivity of Poisson's ratio to uniaxial tensile strain, but it went down with the growth in strain ε_x from 7% to 12%, showing the negative sensitivity of Poisson's ratio to the uniaxial tensile strain. The Al_6MgNb compound possesses the optimal toughness at the uniaxial tensile strain ε_x of 7% because of the largest Poisson's ratio ν value.
4. The Vickers hardness H_V of the Al_6MgNb compound went down rapidly as the uniaxial tensile strain ε_x grew from 0 to 7%, but it changed little as the uniaxial tensile

strain ε_x grew from 7% to 12%. Therefore, the hardness of the Al_6MgNb compound showed negative sensitivity to the uniaxial tensile strain at a strain range of 0–7%.

5. As the uniaxial tensile strain ε_x grew from 0 to 7%, the ratio of the bulk modulus B to the elastic shear modulus G (i.e., B/G) of the Al_6MgNb compound went up, showing positive sensitivity to uniaxial tensile strain, but it decreased with the growth in strain ε_x from 7% to 12%, exhibiting its negative sensitivity to the uniaxial tensile strain. The highest ductility is achieved for the Al_6MgNb compound at the uniaxial tensile strain ε_x of 7% because of the maximum B/G value.
6. The compression anisotropy percentage A_B, shear anisotropy percentage A_G and the universal anisotropy index A_U of the Al_6MgNb compound all increased with the increasing uniaxial tensile strain from 0 to 12%, showing their positive sensitivities to the uniaxial tensile strain. Therefore, the elastic anisotropy was enhanced by the uniaxial tensile strain, and the Al_6MgNb compound exhibited stronger elastic anisotropy at higher uniaxial tensile strain.

Author Contributions: Conceptualization, J.L. and L.L.; methodology, L.Z. and J.Z.; software, L.Z. and Y.L.; validation, L.Z. and Y.L.; formal analysis, L.Z. and J.L.; investigation, L.Z. and J.L.; resources, J.L. and L.L.; data curation, L.Z. and Y.L.; writing—original draft preparation, L.Z. and J.L.; writing—review and editing, J.Z. and L.L.; visualization, L.Z. and Y.L.; supervision, J.L. and J.Z.; project administration, J.L. and J.Z.; funding acquisition, J.L. and L.L. All authors have read and agreed to the published version of the manuscript.

Funding: This research was funded by the Natural Science Foundation of Inner Mongolia Autonomous Region (Grant Nos. 2022MS01009 and 2018MS01013), the Scientific Research Foundation for the High-level Talents of Shanghai Technical Institute of Electronics and Information (Grant No. GCC2024012), the National Natural Science Foundation of China (Grant Nos. 11972221 and 11562016), the College Science Research Project of Inner Mongolia Autonomous Region (Grant No. NJZY22383) and the Key Research Project of Inner Mongolia University of Technology (Grant No. ZZ202016).

Data Availability Statement: Not applicable.

Acknowledgments: We appreciate the technical support from the Mathematics Department of Shanghai Maritime University and the Division of Academic Research of Inner Mongolia Normal University.

Conflicts of Interest: The authors declare no conflict of interest.

References

1. Dolce, D.; Swamy, A.; Hoyt, J.; Choudhury, P. Computing the solid-liquid interfacial free energy and anisotropy of the Al-Mg system using a MEAM potential with atomistic simulations. *Com. Mater. Sci.* **2023**, *217*, 111901. [CrossRef]
2. Mofarrehi, M.; Javidani, M.; Chen, X.-G. Effect of Mn content on the hot deformation behavior and microstructure evolution of Al-Mg-Mn 5xxx alloys. *Mat. Sci. Eng. A* **2022**, *845*, 143217. [CrossRef]
3. Grasserbauer, J.; Weißensteiner, I.; Falkinger, G.; Uggowitzer, P.J.; Pogatscher, S. Influence of Fe and Mn on the microstructure formation in 5xxx alloys-Part II: Evolution of grain size and texture. *Materials* **2021**, *14*, 3312. [CrossRef] [PubMed]
4. Liu, H.; Zhang, Z.; Zhang, D.; Zhang, J. The effect of Ag on the tensile strength and fracture toughness of novel Al-Mg-Zn alloys. *J. Alloys Compd.* **2022**, *908*, 164640. [CrossRef]
5. Thirathipviwat, P.; Nozawa, S.; Furusawa, M.; Onuki, Y.; Hasegawa, M.; Matsumoto, K.; Sato, S. In-situ neutron diffraction study on a dislocation density in a correlation with strain hardening in Al-Mg alloys. *Mat. Sci. Eng. A-Struct.* **2022**, *855*, 143956. [CrossRef]
6. Guo, C.; Zhang, H.T.; Li, J.H. Influence of Zn and/or Ag additions on microstructure and properties of Al-Mg based alloys. *J. Alloys Compd.* **2022**, *904*, 163998. [CrossRef]
7. Xue, D.; Wei, W.; Shi, W.; Guo, Y.W.; Wen, S.P.; Wu, X.L.; Huang, H.; Nie, Z.R. Effect of cold rolling on mechanical and corrosion properties of stabilized Al-Mg-Mn-Er-Zr alloy. *J. Mater. Res. Technol.* **2021**, *15*, 6329–6339. [CrossRef]
8. Stemper, L.; Tunes, M.A.; Paul, O.; Uggowitzer, P.J.; Pogatscher, S. Age-hardening response of AlMgZn alloys with Cu and Ag additions. *Acta Mater.* **2020**, *195*, 541–554. [CrossRef]
9. Su, D.; Zhang, J.; Wang, B. The microstructure and weldability in welded joints for AA 5356 aluminum alloy after adding modified trace amounts of Sc and Zr. *J. Manuf. Process.* **2020**, *57*, 488–498. [CrossRef]
10. Chen, H.M.; Li, X.W.; Chen, Z.P.; Zhang, R.; Ma, X.B.; Zheng, F.; Ma, Z.; Pan, F.C.; Lin, X.L. Investigation on electronic structures and mechanical properties of Nb–doped TiAl2 intermetallic compound. *J. Alloys Compd.* **2019**, *780*, 41–48. [CrossRef]

11. Bao, N.Y.; Tong, Q.C.; Guo, F.Y.; Zhang, S.; Kang, D.D.; Akinpelu, A.; Lv, J.; Yao, Y.S.; Dai, J.Y. Structures and properties of uranium–niobium intermetallic compounds under high pressure: A first principles study. *J. Appl. Phys.* **2023**, *133*, 095901. [CrossRef]
12. Chen, Z.-P.; Ma, Y.-N.; Lin, X.-L.; Pan, F.-C.; Xi, L.-Y.; Ma, Z.; Zheng, F.; Wang, Y.-Q.; Chen, H.-M. Electronic structure and mechanical properties of Nb-doped γ-TiAl intermetallic compounds. *Acta. Phys. Sin.* **2017**, *66*, 196101. [CrossRef]
13. Yang, H.-F.; Chen, T.-H.; Syu, Y.-Y. Mechanical properties and microstructural evolution of TiNi-based intermetallic alloy with Nb addition. *Materials* **2022**, *15*, 3124. [CrossRef] [PubMed]
14. Mahmoodan, M.; Gholamipour, R.; Sohrabi, S. Tuning glass formation and mechanical properties of ZrCoAl(Nb) bulk metallic glass with Nb microalloying Process. *T. Indian I Metals.* **2021**, *74*, 1603–1609. [CrossRef]
15. Dang, C.Q.; Chou, J.-P.; Dai, B.; Chou, C.-T.; Yang, Y.; Fan, R.; Lin, W.T.; Meng, F.; Hu, A.; Zhu, J.; et al. Achieving large uniform tensile elasticity in microfabricated diamond. *Science* **2021**, *371*, 76–78. [CrossRef] [PubMed]
16. Qi, Y.P.; Sadi, M.A.; Hu, D.; Zheng, M.; Wu, Z.P.; Jiang, Y.C.; Chen, Y.P. Recent progress in strain engineering on Van der Waals 2D materials: Tunable electrical, electrochemical, magnetic, and optical properties. *Adv. Mater.* **2023**, *35*, e2205714. [CrossRef] [PubMed]
17. Dong, H.R.; Peng, X.Y.; Wang, H.B.; Fu, L.; Zhao, S.T.; Li, X.Q.; Li, L. An anomalous compression-induced softening behavior of AA6014-T4P during cyclic loading. *Eur. J. Mech. A-Solid.* **2023**, *98*, 104864. [CrossRef]
18. Tan, Y.; Ma, L.M.; Wang, Y.S.; Zhou, W.; Wang, X.L.; Guo, F. Mechanical and thermodynamic behaviors of $AlSi_2Sc_2$ under uniaxial tensile loading: A first-principles study. *J. Phys. Chem. Solids* **2023**, *174*, 111160. [CrossRef]
19. Islam, R.; Mojumder, R.H.; Moshwan, R.; Jannatul Islam, A.S.M.; Islam, M.A.; Rahman, S.; Kabir, H. Strain-driven optical, electronic, and mechanical properties of inorganic halide perovskite $CsGeBr_3$. *ECS J. Solid State Sci. Technol.* **2022**, *11*, 033001. [CrossRef]
20. Sun, B.Z.; Pan, Y.; Yang, J.K.; Guo, J.; Zhao, B.; Liu, X.; Liu, Z.Y.; Li, X.G. Microstructure evolution and SSCC behavior of strain-strengthened 304 SS pre–strained at room temperature and cryogenic temperature. *Corros. Sci.* **2023**, *210*, 110855. [CrossRef]
21. Refson, K.; Tulip, P.R.; Clark, S.J. Variational density-functional perturbation theory for dielectrics and lattice dynamics. *Phys. Rev. B* **2006**, *73*, 155114. [CrossRef]
22. Perdew, J.P.; Burke, K.; Ernzerhof, K.M. Generalized gradient approximation made simple. *Phys. Rev. Lett.* **1996**, *77*, 3865–3868. [CrossRef] [PubMed]
23. Zhu, H.Y.; Shi, L.W.; Li, S.Q.; Zhang, S.B.; Xia, W.S. Effects of biaxial strains on electronic and elastic properties of hexagonal XSi_2 (X = Cr, Mo, W) from first-principles. *Solid State Commun.* **2018**, *270*, 99–106. [CrossRef]
24. Yang, J.Z.; Yang, D.F.; Wang, Y.Q.; Quan, X.J.; Li, Y.Y. First principles investigation of elastic and thermodynamic properties of CoSbS thermoelectric material. *J. Solid State Chem.* **2021**, *302*, 122443. [CrossRef]
25. Born, M.; Huang, K.; Lax, M. Dynamical theory of crystal lattices. *Am. J. Phys.* **1955**, *23*, 474. [CrossRef]
26. Peng, M.J.; Wang, R.F.; Wu, Y.J.; Yang, A.C.; Duan, Y.H. Elastic anisotropies, thermal conductivities and tensile properties of MAX phases Zr_2AlC and Zr_2AlN: A first-principles calculation. *Vacuum* **2022**, *196*, 110715. [CrossRef]
27. Mouhat, F.; Coudert, F.-X. Necessary and sufficient elastic stability conditions in various crystal systems. *Phys. Rev. B* **2014**, *90*, 224104. [CrossRef]
28. Yang, A.C.; Bao, L.K.; Peng, M.J.; Duan, Y.H. Explorations of elastic anisotropies and thermal properties of the hexagonal $TMSi_2$ (TM = Cr, Mo, W) silicides from first-principles calculations. *Mater. Today Commun.* **2021**, *27*, 102474. [CrossRef]
29. Li, L.H.; Wang, W.L.; Wei, B. First-principle and molecular dynamics calculations for physical properties of Ni-Sn alloy system. *Comput. Mater. Sci.* **2015**, *99*, 274–284. [CrossRef]
30. Chen, X.Q.; Niu, H.Y.; Li, D.Z.; Li, Y.Y. Modeling hardness of polycrystalline materials and bulk metallic glasses. *Intermetallics* **2011**, *19*, 1275–1281. [CrossRef]
31. Pugh, S.F. XCII. Relations between the elastic moduli and the plastic properties of polycrystalline pure metals. *Lond. Edinb. Dublin Philos. Mag. J. Sci.* **1954**, *45*, 823–843. [CrossRef]
32. Zhu, H.Y.; Shi, L.W.; Li, S.Q.; Zhang, S.B.; Xia, W.S. Pressure effects on structural, electronic, elastic and lattice dynamical properties of XSi_2 (X=Cr, Mo, W) from first principles. *Int. J. Mod. Phys. B* **2018**, *32*, 1850120. [CrossRef]